HHS Public Access

Author manuscript

Horm Behav. Author manuscript; available in PMC 2022 January 01.

Published in final edited form as:

Horm Behav. 2021 January ; 127: 104888. doi:10.1016/j.yhbeh.2020.104888.

Vasopressin regulates daily rhythms and circadian clock circuits in a manner influenced by sex

Kayla E. Rohr, **Adam Telega**, **Alexandra Savaglio**, **Jennifer A. Evans***

Marquette University, Department of Biomedical Sciences

Abstract

Arginine vasopressin (AVP) is a neurohormone that alters cellular physiology through both endocrine and synaptic signaling. Circadian rhythms in AVP release and other biological processes are driven by the suprachiasmatic nucleus (SCN) of the anterior hypothalamus. Loss of vasopressin signaling alters circadian behavior, but the basis of these effects remains unclear. Here we investigate the role of AVP signaling in circadian timekeeping by analyzing behavior and SCN function in a novel AVP-deficient mouse model. Consistent with previous work, loss of AVP signaling increases water consumption and accelerates recovery to simulated jetlag. We expand on these results to show that loss of AVP increases period, imprecision and plasticity of behavioral rhythms under constant darkness. Interestingly, the effect of AVP deficiency on circadian period was influenced by sex, with loss of AVP lengthening period in females but not males. Examining SCN function directly with *ex vivo* bioluminescence imaging of clock protein expression, we demonstrate that loss of AVP signaling modulates the period, precision, and phase relationships of SCN neurons in both sexes. This pattern of results suggests that there are likely sex differences in downstream targets of the SCN. Collectively, this work indicates that AVP signaling modulates circadian circuits in a manner influenced by sex, which provides new insight into sexual dimorphisms in the regulation of daily rhythms.

Keywords

Vasopressin signaling; suprachiasmatic nucleus; circadian behavior; sex difference; clock circuits

Introduction

Arginine vasopressin (AVP) is an important neurohormone that fluctuates daily due to regulation by the master circadian clock in the suprachiasmatic nucleus (SCN) of the anterior hypothalamus (Schwartz and Reppert, 1985). The SCN is a neural network (Evans, 2016; Hastings et al., 2018) in which cellular rhythms are regulated by transcriptional-translational feedback loops that influence gene expression across the day (Buhr and

*Corresponding author: 560 N 16th St, Schroeder Complex, Room 446, Milwaukee, WI 53233, Phone: 414 288-5732, Fax: 414-288-6564, jennifer.evans@marquette.edu.

Takahashi, 2013; Partch et al., 2014). The core loop of this molecular clock involves the daily activation by CLOCK and BMAL1 of the repressive elements PERIOD and CRYPTOCHROME, which operates in nearly all cells of the body to regulate >40% of protein-coding genes in a tissue-specific manner (Zhang et al., 2014). Although molecular clock function is observed in all tissues, the SCN is unique in that its cells communicate with one another to determine emergent properties of the network. For example, dissociated SCN neurons show large differences in cellular period (Welsh et al., 1995), but coupled SCN neurons adopt a common period (Low-Zeddies and Takahashi, 2001; Smyllie et al., 2016) that ensures the fidelity of output signals and expression of rhythms at the overt level. In addition, coupled SCN neurons display more precise and higher amplitude rhythms than isolated SCN neurons (Herzog et al., 2004; Webb et al., 2009), which ensures daily rhythms are reliable from cycle to cycle (i.e., precise) and less sensitive to external perturbation (i.e., more robust). Finally, SCN neurons adopt specific phase relationships that encode salient features of the environment, such as seasonal changes in day length (Evans and Gorman, 2016; Meijer et al., 2010) to maintain temporal homeostasis. Given its importance for circadian timekeeping, defining the signals and circuits by which SCN cells communicate remains important for understanding the daily control of biological processes in mammals.

Arginine vasopressin (AVP) is an important SCN output that regulates downstream tissues (Groblewski et al., 1981; Kalsbeek et al., 2010). AVP signaling also influences SCN function directly through mechanisms that remain poorly understood. For instance, mice lacking the AVP receptors V1A and V1B recover faster from simulated jetlag, with accelerated re-entrainment of daily rhythms in locomotion, body temperature, and molecular clock function in both the SCN and the liver (Y amaguchi et al., 2013). Consistent with a local role for AVP signaling, V1A and V1B are both expressed in the SCN, and V1A/B antagonism modulates molecular rhythms in *ex vivo* SCN slice preparations (Bedont et al., 2018; Edwards et al., 2016). Further, genetic modulation of the molecular clock specifically in AVP-expressing SCN neurons can be transmitted to the entire system to regulate the expression of daily rhythms in mice (Mieda et al., 2016; Mieda et al., 2015). Overall, these results suggest that AVP signaling influences the function of both the SCN and its downstream targets, which dovetails with known effects of AVP signaling in other hypothalamic structures (Ludwig, 1998).

Given renewed appreciation that AVP may directly modulate SCN network properties, here we test the role of AVP in regulating clock function using a novel AVP-deficient mouse model (Cheng et al., 2019). We confirm loss of AVP, increased water intake, and accelerated recovery to simulated jetlag in this mouse model. By examining effects on free-running rhythms that reflect intrinsic clock function, we further demonstrate that loss of AVP signaling in this model also alters the period, precision, and plasticity of circadian rhythms in a sex-influenced manner. Using *ex vivo* real-time bioluminescence imaging of clock protein expression, we show that loss of AVP signaling alters SCN period, precision, and organization. Overall, this work provides novel insights into the role of AVP signaling in circadian circuits by revealing local and systemic effects that vary by sex.

Methods

Mice and husbandry conditions

Mice were bred and raised under a 24-hour light-dark cycle with 12 hours of light and 12 hours of darkness [LD12:12; lights-off at 1800 CST, defined as Zeitgeber Time 12 (ZT12), 10-30 lux]. Throughout life, ambient temperature was maintained at 22°C ± 2°C, with *ad libitum* access to water and food (Teklad Rodent Diet 8604). Founder heterozygous *Avp*-IRES2-Cre-D mice (Harris et al., 2014) were obtained from Jackson Laboratory (B6.Cg-*Avp*$^{<tm1.1(cre)Hze>}$/J; Stock No: 023530) and bred to PERIOD2::LUCIFERASE (PER2::LUC) mice (Yoo et al., 2004) across multiple generations to produce homozygous AVP-IRES-Cre mice (*Avp*$^{cre/cre}$), heterozygous AVP-IRES-Cre mice (*Avp*$^{cre/+}$), and wild-type mice (*Avp*$^{+/+}$). At weaning, mice were group housed in same-sex cages without running wheels. Although genotyping protocols supplied by the vendor were unable to distinguish between *Avp*$^{cre/cre}$ and *Avp*$^{cre/+}$ mice, detection of homozygosity was obtained using a commercial assay (Transnetyx, Inc; Cordova, TN, USA) of Cre expression levels using qPCR (Primers: Forward- TTAATCCATATTGGCAGAACGAAAACG, Reverse-CAGGCTAAGTGCCTTCTCTACA). Importantly, Cre expression levels correlated with AVP levels in post mortem tissues (Spearman's Rho: $r = 0.89$, $p < 0.001$). All procedures were conducted according to the National Institutes of Health Guide for the Care and Use of Animals and were approved by the Institutional Animal Care and Use Committee at Marquette University.

Immunohistochemistry

To assess whether Cre interferes with neuropeptide expression, brains were collected from male and female *Avp*$^{cre/cre}$, *Avp*$^{cre/+}$, and *Avp*$^{+/+}$ mice. Mice were deeply anesthetized with isoflurane and sacrificed by cervical dislocation. In P21 mice, brains were collected at ZT12 (n = 6-10/genotype). In adult mice (23-25 weeks old, n = 9-12/genotype/sex), brains were collected 48 h after 1μl colchicine injection into the third ventricle (0.5μl/min) to assess total peptide expression over the circadian cycle. After collection, brains were fixed in 4% paraformaldehyde for 18-20 h, cryoprotected in 20% sucrose for 3 days, and then sectioned with a cryostat in the coronal plane. Free-floating SCN slices (40μm) were processed for AVP- and VIP-immunoreactivity, as described in (Bedont et al., 2018). Briefly, slices were rinsed in PBS, incubated for 48 h in primary antibodies (guinea pig anti-AVP, 1:1000, Peninsula, Cat# T-5048; rabbit anti-VIP, 1:500, Peninsula, Cat# T-4246), rinsed again in PBS, incubated for 2 h in secondary antibodies (donkey anti-guinea pig Alexa 594, Jackson, Cat# 706-585-148; donkey anti-rabbit Alexa 488, Jackson, Cat# 711-545-152, both at 1:200), then rinsed a final time in PBS. Slices were mounted onto microscope slides in Prolong Anti-Fade mounting medium with DAPI (Invitrogen, Cat# P36935) before coverslipping. Fluorescent images were collected on a Nikon 80i microscope fitted with a Retiga 2000R digital camera (QImaging, Surrey, BC, Canada) connected to a computer running NIS Elements-D software (Nikon Instruments, Melville NY, USA) then analyzed using ImageJ software. Background subtraction was performed using signal intensity from adjacent non-SCN tissue.

Behavioral analyses

To evaluate drinking levels, nighttime water consumption was tracked in male and female mice of each genotype (15-22 weeks old, n = 2-5/genotype/sex) for 7 consecutive days. To evaluate genotype differences in locomotor activity rhythms, $Avp^{cre/cre}$, $Avp^{cre/+}$, and $Avp^{+/+}$ mice (10-18 weeks old, n = 9-12/genotype/sex) were individually housed in running-wheel cages under LD12:12 for 4 weeks (lights-off at 1800 CST, white LEDs: 150 ± 30 lux), then exposed to simulated jetlag by advancing the LD cycle by 6 h (LD shift, new lights-off: 1200 CST). Mice were relatively undisturbed for 4 weeks except for routine husbandry, then released into constant darkness (DD) for at least 3 weeks. After DD, mice were re-entrained to LD12:12 for at least 14 days prior to colchicine injection and brain collection. Wheelrunning data were collected and analyzed with ClockLab software (Actimetrics, Wilmette, IL). The time of activity onset and offset was determined for each day of the experiment. For jetlag recovery, the average time of activity onset under baseline conditions was calculated, which was compared to the time of activity onset on each day after the shift in the light:dark cycle. Recovery from simulated jetlag was quantified for each mouse by calculating the number of days required to advance activity onset by 6 h (i.e., align to new lights-off) and maintain this new phase for at least 4/6 days thereafter. Free-running period in DD was quantified using a linear regression fit to activity onsets or activity offsets over 28 days after release. Precision of the free-running rhythm was quantified as the inverse of the error associated with the linear regression of activity onsets. Lastly, effects on the waveform of the activity rhythms was investigated by calculating the duration of the active phase by quantifying the temporal difference between activity offset and onset on each day of the experiment.

Tissue collection and ex vivo assays

To test genotype effects on master clock function, coronal SCN slices (150μm) were collected from male and female $Avp^{cre/cre}$, $Avp^{cre/+}$, and $Avp^{+/+}$ mice (10-20 weeks old) and cultured as described previously (Bedont et al., 2018). Mice were anesthetized with isoflurane and sacrificed using cervical dislocation 4-6 h before lights off (Davidson et al., 2009). Three consecutive SCN slices were collected using a vibratome (Leica VT1200S) and trimmed by hand under a dissecting microscope. SCN slices were cultured at 37°C on a membrane insert in a dish containing 1.2mL of air-buffered Dulbecco's modified explant medium (DMEM, Sigma D2902) supplemented with 0.1mM beetle luciferin, 0.02% B27 (Gibco 17504), 0.01% HEPES (Gibco 15630), 0.005% $NaCHO_3$ (Gibco 25080), 0.004% Dextrose (Sigma G7021), and 0.01% penicillin/streptomycin (Gibco 15140). Cellular bioluminescence rhythms were imaged using a Stanford Photonics XR Mega 10z CCD camera mounted onto a Zeiss Axio Observer Z1 microscope controlled with Piper software (Stanford Photonics). Images (1.4k×1k 16-bit) were collected at 15 frames/sec, filtered in real-time to eliminate single-image noise events (i.e., cosmic rays), and stored as 2 min-summed images collected once every 10 min. A 2 h moving average was then applied (Piper Software), images were converted to 8-bit, pixel dimensions were reduced in half, and three consecutive images were summed to produce a series of 30 min images (ImageJ Software). Last, to test the efficacy of Cre-induced transduction, SCN slices were collected from P21 $Avp^{cre/cre}$, $Avp^{cre/+}$, and $Avp^{+/+}$ mice (n = 2-6/genotype) and cultured with AAV8-FLEX-tdTomato (University of North Carolina Vector Core, Cat# AV4912b). To assess transduction

efficiency *in vitro*, tdTomato expression was imaged weekly for 4 weeks on a Nikon confocal microscope Al (Nikon Instruments, Melville, NY) and tdT+ cells were counted using ImageJ software.

PER2::LUC analyses

Recording start time for each sample was expressed relative to the Zeitgeber Time to normalize time *in vitro* across samples. Matlab-based computational analyses were used to analyze SCN cellular rhythms, as in previous work (Evans et al., 2011, 2013). To locate and extract data from cell-like ROIs, an iterative process was employed after background and local noise subtraction. For each cell-like ROI, we calculated the phase of peak PER2::LUC on the first cycle *in vitro*, average period across the first three cycles in vitro, precision of cellular period (i.e., inverse of the standard deviation in cycle-to-cycle period length), and damping of cellular amplitude (i.e., amplitude of Cycle3/Cyclel).

Statistical analyses

Data are represented in figures and tables as mean ± SEM. Statistical analyses were performed with JMP software (SAS Institute, Cary, NC) and circular statistics were performed using Oriana software (Kovach Computing Services, Anglesey Wales). Full Factorial ANOVA was used to assess behavioral effects of Genotype, Sex, and Genotype*Sex interaction, followed by post hoc Feast Square Means (LSM) Contrasts. Also, full factorial ANOVA was used to assess SCN effects of Genotype, Sex, Slice/Region, and Genotype* Sex, Genotype*Slice/Region, Sex*Slice/Region, and the Genotype*Sex*Slice/Region interaction, followed by post hoc LSM Contrasts. Further, one-way ANOVA was conducted after dividing by sex, genotype or slice/peptide where appropriate, using post hoc Tukey's HSD to control for family-wise error. Changes in behavior and SCN function over time were analyzed with Repeated Measures MANOVA, followed by post hoc Full Factorial ANOVA and LSM Contrasts. Spearman's Rho was used to correlate levels of AVP with circadian behavior. Statistical significance was set at $p < 0.05$, and effect sizes were estimated by calculating the values of partial η^2 ($SS_{effect}/SS_{effect}+SS_{error}$) and Cohen's d ($M_1$-$M_2/s_{pooled}$) where appropriate.

Results

Decreased AVP expression and increased water consumption in $Avp^{cre/cre}$ mice.

Levels of AVP were decreased in the paraventricular nucleus (PVN) and supraoptic nucleus (SON) by 75% in adult $Avp^{cre/cre}$ mice and 20-40% in $Avp^{cre/+}$ mice of both sexes (Figure 1A–B, Table S1, Figure S1, Genotype: $p < 0.001$, Sex: $p > 0.1$, LSM Contrasts: $Avp^{+/+}$ vs. $Avp^{cre/+}$ $p < 0.05$, $d > 0.89$, $Avp^{+/+}$ vs. $Avp^{cre/cre}$ $p < 0.0001$, $d > 2.09$). AVP deficiency was likewise detected earlier in development at P21 (Figure S1, Genotype: $p < 0.005$, LSM Contrasts: $Avp^{+/+}$ vs. $Avp^{cre/+}$ $p < 0.05$, $d > 1.31$, $Avp^{+/+}$ vs. $Avp^{cre/cre}$ $p < 0.005$, $d > 2.42$). Consistent with previous work in other AVP-deficient models (Groblewski et al., 1981), water consumption was elevated in $Avp^{cre/cre}$ mice (Figure 1C, Genotype: $p < 0.0001$, LSM Contrast: $p < 0.0001$, $d = 7.98$), with higher drinking levels in female $Avp^{cre/cre}$ mice relative to male $Avp^{cre/cre}$ mice (Sex: $p < 0.05$, LSM Contrast: $p < 0.05$, $d = 1.94$). In adult mice, body weight did not differ across groups in either sex (Table S2, Genotype: $p > 0.1$). Fast,

DAPI staining did not differ by genotype in either structure at either age (Figure S1, Genotype: $p > 0.1$), suggesting that Cre did not suppress AVP expression via apoptosis (Rezai Amin et al., 2019).

In the adult SCN, AVP was likewise decreased in a Cre copy dependent manner (Figure 2A–B, Table S1, Genotype: $p < 0.0001$, LSM Contrasts: $Avp^{+/+}$ vs. $Avp^{cre/+}$ $p < 0.0001$, $d = 2.31$, $Avp^{+/+}$ vs. $Avp^{cre/cre}$ $p < 0.0001$, $d = 6.17$). At P21, AVP was decreased in $Avp^{cre/cre}$ mice only (Figure S2A, Genotype: $p < 0.001$, LSM Contrast: $p < 0.0001$, $d = 3.46$), thus differing from the pattern observed in PVN and SON at this age. SCN VIP and DAPI staining was not significantly decreased at either age, although there was a trend for increased DAPI in the adult $Avp^{cre/cre}$ SCN (Figure 2C, Figure S2A). Further, Cre recombinase expression was sufficient to transduce SCN neurons *ex vivo* collected from both $Avp^{cre/cre}$ and $Avp^{cre/+}$ P21 mice (Figure S2B–C, Genotype: $p < 0.05$, LSM Contrasts: $Avp^{+/+}$ vs. $Avp^{cre/+}$ $p < 0.001$, $d > 4.86$, $Avp^{+/+}$ vs. $Avp^{cre/cre}$ $p < 0.005$, $d > 2.19$). Collectively, these data indicate that the Cre transgene interferes with AVP expression in both $Avp^{cre/cre}$ and $Avp^{cre/+}$ mice, which extends previous work (Cheng et al., 2019).

Circadian behavior is altered in $Avp^{cre/cre}$ mice in a manner influenced by sex.

Next we tested whether AVP-IRES-Cre mice would adjust faster to simulated jetlag (Figure 3A), similar to $V1a^{-/-}V1b^{-/-}$ mice (Yamaguchi et al., 2013). Baseline entrainment did not differ by genotype (Table S2, Genotype: $p > 0.1$), although wheel-running levels were reduced in male $Avp^{cre/cre}$ mice relative to $Avp^{+/+}$ males (Table S2, Genotype: $p < 0.05$, LSM Contrast: $p < 0.05$, $d = 0.85$). Sex differences were evident in wheel-running levels, the time of activity offset, and activity duration (Table S2, Sex: $p < 0.005$, LSM Contrasts: $p < 0.05$, $d > 0.89$). After the 6 h shift of the light:dark cycle, $Avp^{+/+}$ mice required ca. 8 days to re-entrain, while $Avp^{cre/+}$ and $Avp^{cre/cre}$ mice recovered in 6 and 5 days, respectively (Figure 3B, Genotype: $p < 0.0001$, LSM Contrasts: $Avp^{+/+}$ vs. $Avp^{cre/+}$ $p < 0.05$, $d = 0.85$, $Avp^{+/+}$ vs. $Avp^{cre/cre}$ $p < 0.001$, $d = 1.35$). Consistent with previous work (Feillet et al., 2016), female $Avp^{+/+}$ mice recovered faster than their male cohorts (Figure 3B, Sex: $p < 0.05$, LSM Contrast: $p < 0.05$, $d = 0.85$). However, reentrainment did not differ by sex in each mutant group (Figure 3B, LSM Contrasts: $p > 0.1$, $Avp^{cre/+}$ $d = 0.69$, $Avp^{cre/cre}$ $d = 0.33$). In both sexes, accelerated recovery in $Avp^{cre/cre}$ and $Avp^{cre/+}$ mice was driven by larger phase shifts on the first few days after the shift (Figure S3A, Genotype: $p < 0.001$, LSM Contrasts: $Avp^{+/+}$ vs. $Avp^{cre/+}$ $p < 0.05$, $d = 0.63$-1.00, $Avp^{+/+}$ vs. $Avp^{cre/cre}$ $p < 0.05$, $d = 0.55$-0.76). As expected, AVP levels were correlated with re-entrainment rate, with lower AVP expression associated with a faster jetlag recovery time in both sexes (Figure S3B, $p < 0.001$). These data indicate that loss of AVP in AVP-IRES-Cre mice decreases circadian robustness, similar to $V1a^{-/-}V1b^{-/-}$ mice (Yamaguchi et al., 2013).

Next we examined changes in intrinsic circadian timekeeping by assessing the period, precision, and waveform of wheel-running rhythms under constant darkness (Figure 4A). Genotype influenced free-running period in a manner dependent on sex (Figure 4B, Genotype: $p < 0.005$, Genotype*Sex: $p < 0.05$). Specifically, female $Avp^{cre/cre}$ mice adopted a longer period than their same-sex cohorts (Figure 4B, LSM Contrasts: $Avp^{cre/cre}$ vs. $Avp^{+/+}$ $p = 0.0001$, $d = 2.04$, $Avp^{cre/cre}$ vs. $Avp^{cre/+}$ $p = 0.005$, $d = 1.35$). In contrast, period did

not differ by genotype in males (Figure 4B, LSM Contrasts: $p > 0.1$, $d < 0.35$). Consequently, female $Avp^{cre/cre}$ mice displayed a longer period than male $Avp^{cre/cre}$ mice (Figure 4B, LSM Contrast: $p = 0.02$, $d = 0.95$). Further, $Avp^{cre/cre}$ mice had less precise locomotor rhythms (Figure 4C, Genotype: $p < 0.005$, LSM Contrast: $p < 0.05$, $d = 1.11$) with higher plasticity in waveform due to greater expansion of the active phase over time in constant darkness (Figure 4D, Genotype: $p < 0.01$, LSM Contrast: $p < 0.05$, $d = 0.86$). Reduced precision and greater plasticity was observed in $Avp^{cre/cre}$ mice of both sexes, nevertheless sex influenced phenotypic differences in both measures (Figure 4C–D, Figure S4). For example, circadian waveform differed by the first week in female $Avp^{cre/cre}$ mice, but not male $Avp^{cre/cre}$ mice (Figure S4, LSM Contrast: female $Avp^{+/+}$ vs. female $Avp^{cre/cre}$ $p < 0.05$, $d = 1.36$). As such, female $Avp^{cre/cre}$ mice displayed greater expansion of activity duration than male $Avp^{cre/cre}$ mice during the first week of constant darkness (Figure S4, LSM Contrast: $p < 0.05$, $d = 0.95$). In addition, male $Avp^{cre/+}$ mice displayed more expansion of circadian waveform over time in DD relative to male $Avp^{+/+}$ mice and female $Avp^{cre/+}$ mice (Figure S4, LSM Contrasts: male $Avp^{+/+}$ vs. male $Avp^{cre/+}$ $p < 0.05$, $d = 1.15$, male $Avp^{cre/+}$ vs. female $Avp^{cre/+}$ $p < 0.05$, $d = 0.92$). Lastly, precision was lower in female $Avp^{cre/+}$ relative to male $Avp^{cre/+}$ mice (Figure 4C, LSM Contrast: $p < 0.05$, $d = 1.13$). Importantly, post mortem SCN AVP levels were correlated with behavioral period, precision, and plasticity (Figure S3C–E), suggesting loss of AVP signaling modulates intrinsic circadian function by affecting the SCN and/or its downstream targets.

Neurobiological correlates of behavior indicate AVP influences the SCN and circadian system

To test if changes in circadian behavior reflected altered SCN function, we imaged PER2::LUC rhythms in SCN neurons collected from adult wild-type and AVP-IRES-Cre mice (Figure 5). Compared to $Avp^{+/+}$ SCN, the period of PER2::LUC rhythms was longer in $Avp^{cre/+}$ and $Avp^{cre/cre}$ SCN neurons of both sexes (Figure 6A, Genotype: $p < 0.01$, LSM Contrasts: $Avp^{+/+}$ vs. $Avp^{cre/+}$ $p < 0.05$, $d = 1.21$, $Avp^{+/+}$ vs. $Avp^{cre/cre}$ $p < 0.05$, $d = 1.1$). Relative to $Avp^{+/+}$ SCN, cellular period was lengthened in $Avp^{cre/cre}$ SCN across the anteroposterior axis (Figure 6B, LSM Contrasts: Anterior SCN $p = 0.05$, $d = 1.2$, Middle SCN $p = 0.02$, $d = 1.1$, Posterior SCN $p = 0.01$, $d = 1.01$). Further, $Avp^{cre/+}$ mice displayed longer period in both the anterior and middle SCN compared to $Avp^{+/+}$ mice (Figure 6B, LSM Contrasts: Anterior SCN $p < 0.005$, $d = 1.4$, Middle SCN $p < 0.005$, $d = 1.5$). Consistent with these network-spanning effects, period was lengthened in each peptide region in $Avp^{cre/+}$ and $Avp^{cre/cre}$ SCN slices (Figure 6C, Genotype: $p < 0.001$. LSM Contrasts: $Avp^{+/+}$ vs. $Avp^{cre/+}$ $p < 0.05$, $d > 0.97$, $Avp^{+/+}$ vs. $Avp^{cre/cre}$ $p < 0.05$, $d > 0.83$). Anteroposterior effects were consistent across male and female SCN (Figure 6B, Sex: $p > 0.1$), but results across peptidergic regions were subtly influenced by sex (Figure S5A). Together, these results indicate that AVP signaling acts to shorten the period of SCN neurons located throughout the network.

Similar to effects on behavior, the precision of PER2::LUC rhythms was decreased in $Avp^{cre/cre}$ SCN neurons in both sexes (Figure 6D, Genotype: $p < 0.05$, Sex: $p > 0.1$, LSM Contrast: $p < 0.05$, $d = 1.2$). In $Avp^{+/+}$ neurons, precision varied across the anteroposterior SCN, being highest in posterior SCN neurons and lowest in the anterior SCN (Figure 6E,

Slice Position: $p < 0.001$, LSM Contrasts: $p < 0.05$, $d > 1.01$). Relative to $Avp^{+/+}$ neurons, $Avp^{cre/cre}$ neurons were less precise in the anterior and middle SCN (Figure 6E, LSM Contrasts: Anterior SCN $p < 0.05$, $d = 0.8$, Middle SCN $p = 0.059$, $d = 1.04$), with significant effects observed in AVP- and VIP-expressing regions (Figure 6F, LSM Contrasts: $p < 0.05$, $d > 0.61$). Anteroposterior effects were consistent across male and female SCN (Figure 6E, Sex: $p > 0.1$), but results across peptidergic regions were influenced by sex (Figure S5B). Consistent with regional differences in precision, damping varied across the anteroposterior axis in the $Avp^{+/+}$ SCN, with posterior SCN neurons damping the least (Figure S6, Slice Position: $p < 0.05$, LSM Contrasts: $p < 0.05$, $d > 1.25$). Consistent with effects on precision, $Avp^{cre/cre}$ SCN neurons displayed increased damping of PER2::LUC rhythms, which interacted with sex (Figure S6, Genotype: $p > 0.1$, Genotype*Sex: $p < 0.05$). Together, these results indicate that AVP signaling acts to modulate precision and damping of SCN neurons in specific subregions of the network.

In addition to effects on period and precision, the organization of the $Avp^{cre/cre}$ SCN network was altered. To investigate network organization, we quantified cellular relationships using the peak time of PER2::LUC expression on the first cycle *ex vivo*. Using a measure of standard deviation that accounts for the circular nature of time, we found greater phase dispersion in $Avp^{cre/cre}$ SCN of both sexes (Figure 7A, Genotype: $p < 0.005$, Sex: $p > 0.1$, LSM Contrast: $p < 0.05$, $d = 1.33$). In $Avp^{+/+}$ SCN, phase dispersion varied across the anteroposterior axis, with the highest phase dispersion in the anterior SCN (Figure 7B, Slice Position: $p < 0.0001$, LSM Contrasts: $p < 0.05$, $d > 1.79$). Relative to $Avp^{+/+}$ SCN, $Avp^{cre/cre}$ SCN had greater phase dispersion in the anterior and middle SCN (Figure 7B, LSM Contrasts: $p < 0.05$, $d > 0.97$), with larger dispersion in both AVP- and VIP-expressing regions (Figure 7C, LSM Contrasts: $p < 0.05$, $d > 0.92$). Anteroposterior effects of $Avp^{cre/cre}$ tended to be higher in female SCN slices (Figure 7B, Sex: $p = 0.056$). Further, greater phase dispersion was observed in female $Avp^{cre/cre}$ SCN over time *ex vivo* (Figure 7D–E, Genotype: Male- $p > 0.1$, Female- $p < 0.005$, LSM Contrasts: $p < 0.05$, $d > 0.95$), and effects of $Avp^{cre/cre}$ across peptidergic regions were specific to females (Figure S5C, Sex: $p < 0.05$, LSM Contrasts: $p < 0.05$, $d > 2.28$). Together, these results indicate that AVP signaling regulates cellular relationships across the SCN network in a manner influenced by sex.

Discussion

Consistent with previous work (Cheng et al., 2019), AVP is reduced in the hypothalamus of AVP-IRES-Cre mice. Confirming loss of AVP, $Avp^{cre/cre}$ mice exhibit increased water consumption and accelerated recovery from simulated jetlag, similar to other AVP-deficient models (Groblewski et al., 1981; Yamaguchi et al., 2013). Building on these results, we provide evidence that AVP influences circadian behavior in three novel ways (i.e., changes in period, precision, and waveform) in a manner influenced by sex. By investigating how these behavioral phenotypes relate to changes in SCN function, this work provides new insight into the role of AVP signaling within the master clock and the larger circadian system.

Effects on water consumption and jetlag recovery support the conclusion that AVP is reduced in $Avp^{cre/cre}$ mice. While $Avp^{cre/+}$ mice did not increase their water intake, AVP was

partially reduced in *Avp*$^{cre/+}$ in the PVN and SON in both sexes and at both ages examined here. Replicating previous work (Yamaguchi et al., 2013), we find that loss of AVP signaling in AVP-IRES-Cre mice modulates adjustment to a new time zone. Unlike effects on water consumption, AVP-IRES-Cre mice recovered faster to simulated jetlag in proportion to Cre dosage. Inclusion of this jetlag assay in the present study adds to previous work that only assayed male *Avp*$^{cre/+}$ mice (Cheng et al., 2019). Effects of Cre insertion on the rate of jetlag recovery likely reflect loss of AVP in the SCN, but downstream tissues may also contribute to this behavioral response. Supporting the importance of SCN AVP signaling, jetlag recovery is accelerated by SCN-specific injections of V1A/B antagonists (Yamaguchi et al., 2013). Further, V1A and V1B signaling contribute additively to jetlag responses (Yamaguchi et al., 2013), and both receptors are expressed in the murine SCN (Bedont et al., 2018). Although female Brattleboro rats lacking AVP do not display faster jetlag recovery (Groblewski et al., 1981), this may reflect a difference in species, experimental design, or nature of the mutation. Unlike many other models, Cre-induced AVP deficiency in the SCN appears to progressively worsen with age, which may be an important distinction given that AVP modulates SCN function across postnatal development (Ono et al., 2016). Site-specific knockdown in future work is needed to test the role of AVP across age, as done recently for VIP (Mazuski et al., 2020). Also, it may be of interest to assess how AVP contributes to circadian robustness and encoding in other entrainment assays potentially mediated by mechanisms distinct from those involved in jetlag recovery.

We also find that *Avp*$^{cre/cre}$ mice of both sexes display reduced precision and increased expansion of the active phase under free-running conditions. AVP signaling influences precision and/or waveform of behavioral rhythms in female Brattleboro rats (Groblewski et al., 1981), male and female *V1a*$^{-/-}$ mice (Li et al., 2009) and male *Avp-Bmal1*$^{-/-}$ mice (Mieda et al., 2015). Much like that observed for free-running behavioral rhythms, the precision of PER2::LUC rhythms in the SCN was decreased in *Avp*$^{cre/cre}$ mice of both sexes. Further, cellular damping of PER2::LUC rhythms was higher in female *Avp*$^{cre/cre}$ mice, consistent with findings that V1A/B antagonists increase damping of PER2::LUC rhythms in organotypic SCN slices (Maywood et al., 2011). The mechanisms underlying this effect remain unclear, but may reflect a direct or indirect effect on the molecular circadian clock. For instance, AVP-deficient Brattleboro rats display lower amplitude of SCN electrical rhythms due to reduced spontaneous firing during the daytime (Ingram et al., 1996), and reduced electrical activity can suppress molecular clock function (Yamaguchi et al., 2003). In addition, we find greater phase dispersion among SCN neurons in *Avp*$^{cre/cre}$ slices, which can modulate circadian waveform at the behavioral level (Evans and Gorman, 2016; Meijer et al., 2010). Thus, loss of AVP signaling may influence plasticity of behavioral waveform under DD via changes in SCN organization and/or cellular coupling. Because *V1a*$^{-/-}$*V1b*$^{-/-}$ mice display deficits in SCN communication after cycloheximide exposure (Y amaguchi et al., 2013), it would be of interest to test whether the loss of AVP signaling influences other measures of SCN coupling (Evans et al., 2013). Collectively, the current results suggest that AVP acts locally within the SCN itself to modulate cellular precision and network organization in both sexes, although this does not exclude the possibility that AVP signaling also regulates these properties in downstream clock tissues.

Of the novel results found here, we demonstrate loss of AVP signaling lengthens circadian period specifically in female $Avp^{cre/cre}$ mice. Longer period due to AVP deficiency is consistent with results found in work using female Brattleboro rats (Groblewski et al., 1981) male and female $V1a^{-/-}$ mice (Li et al., 2009) and male mice (Mieda et al., 2015), but not other work using male rats and mice (Bult et al., 1993; Yamaguchi et al., 2013). Free-running period did not differ by sex in $Avp^{+/+}$ mice in agreement with previous work (Brockman et al., 2011; Iwahana et al., 2008; Kuljis et al., 2013). Nevertheless, sex-specific effects of AVP deficiency suggest that cellular mechanisms regulating this circadian property differ in males and females. The SCN may not be the locus of this effect since the period of SCN PER2::LUC rhythms was longer in $Avp^{cre/cre}$ and $Avp^{cre/+}$ mice of both sexes, although this assay indexes only one component of master clock function. Consistent with effects of AVP-IRES-Cre on SCN PER2::LUC rhythms observed here, V1A/B antagonists increase the period of PER2::LUC rhythms in SCN collected from both male and female mice (Bedont et al., 2018). Discrepant effects of AVP-IRES-Cre on behavioral versus SCN period suggest that loss of AVP signaling may induce sex-specific compensatory mechanisms in downstream tissues (Abrahamson and Moore, 2001; Rood et al., 2013; Vida et al., 2010). Notably, recent work suggests that AVP neurons in non-SCN tissues play sexually dimorphic roles in the regulation of social, affective, and sickness behaviors (Rigney et al., 2020a; Rigney et al., 2020b; Rigney et al., 2019; Whylings et al., 2020). That neural circuits and functional consequences differ by sex highlights the need for more routine inclusion of female subjects in biomedical research (Beery and Zucker, 2011; Prendergast et al., 2014).

Sex and gonadal steroids can influence circadian behavior, but many of these effects are not consistent across species and studies (Krizo and Mintz, 2014). Female $Avp^{+/+}$ mice in the present study adjusted to jetlag faster than their male cohorts, consistent with previous work (Feillet et al., 2016). The neural mechanisms underlying these effects remain unclear. Female mice do not display larger phase advances than male mice in response to discrete light pulses (Blattner and Mahoney, 2013; Brockman et al., 2011), but gonadal hormones and sex chromosome can modulate photic responses in both sexes (Blattner and Mahoney, 2012; Brockman et al., 2011; Karatsoreos et al., 2011; Kuljis et al., 2013; Royston et al., 2014). This indicates that further work investigating behavioral and cellular responses to light in both sexes may reveal novel cellular mechanisms regulating circadian robustness. Interestingly, loss of AVP equalized the rate of jetlag recovery across sex, but AVP levels did not differ between males and females presently. Further, daily rhythms in *Avp* mRNA expression in the SCN do not differ by sex in nocturnal and diurnal rats (Krajnak et al., 1998; Mahoney et al., 2009), but sex differences in V1A/B expression and/or receptor signaling have not been examined. Loss of AVP also influenced precision and waveform under free-running conditions, but these measures did not differ by sex in $Avp^{+/+}$ or $Avp^{cre/cre}$ mice. Nevertheless, $Avp^{cre/+}$ mice displayed sex-influenced results for both parameters, which suggests sexual dimorphism in the sensitivity to partial AVP deficiency. Previous work has suggested that sex and/or gonadal hormones can modulate circadian precision and waveform (Iwahana et al., 2008; Kuljis et al., 2013; Royston et al., 2014), but inconsistencies across studies preclude understanding the precise underlying mechanisms. Because biological sex is not explicitly included as a variable in many circadian studies

(Kuljis et al., 2013), it is possible that sex differences in cellular mechanisms regulating clock function has been overlooked in past work.

Conclusions

Insertion of the Cre transgene decreases AVP expression in the hypothalamus of AVP-IRES-Cre mice, which should be considered when using this model. Here we use this AVP-deficient mouse model to replicate previous work and demonstrate novel effects of AVP on circadian behavior that correspond to changes in SCN function. Further, we find that loss of AVP influenced circadian behavior and clock function in a manner influenced by biological sex. Wildtype male and female mice did not differ in SCN PER2::LUC rhythms for any of the parameters investigated here, consistent with previous work (Kuljis et al., 2013). Nevertheless, loss of AVP expression modulated SCN PER2::LUC rhythms by affecting cellular clock function in specific regions dependent on sex. These results illustrate how neural circuits may be constructed differently in males and females to achieve similar behavioral and cellular outputs under standard physiological conditions. Going forward, there is a need for studies investigating circadian circuitry using wildtype and mutant models to include both males and females. These future studies have potential to provide further insight into sex-specific circuits in the master clock and the larger circadian system.

Supplementary Material

Refer to Web version on PubMed Central for supplementary material.

Acknowledgements

We would like to thank Thomas Inda and Harshida Pancholi for their assistance in executing these experiments. We are grateful to Alec Huber, Austin Fritsch, Alecia Bjerke, Erika Johnson, Audrey Konieczny, and Berri Foreman for animal care. Also, we would like to thank Stanford Photonics for their equipment and technical assistance. The National Institutes of Health (R01091234), the Whitehall Foundation (2014-12-65), and the Charles E Kubly Mental Health Research Center supported this work. The authors have no potential conflicts of interest with respect to the research, authorship, and/or publication of this article.

References

Abrahamson EE, Moore RY, 2001 Suprachiasmatic nucleus in the mouse: Retinal innervation, intrinsic organization and efferent projections. Brain Res 916, 172–191. [PubMed: 11597605]

Bedont JL, Rohr KE, Bathini A, Hattar S, Blackshaw S, Sehgal A, Evans JA, 2018 Asymmetric vasopressin signaling spatially organizes the master circadian clock. J Comp Neurol 526, 2048–2067. [PubMed: 29931690]

Beery AK, Zucker I, 2011 Sex bias in neuroscience and biomedical research. Neurosci Biobehav Rev 35, 565–572. [PubMed: 20620164]

Blattner MS, Mahoney MM, 2012 Circadian parameters are altered in two strains of mice with transgenic modifications of estrogen receptor subtype 1. Genes Brain and Behavior 11, 828–836.

Blattner MS, Mahoney MM, 2013 Photic phase-response curve in 2 strains of mice with impaired responsiveness to estrogens. J Biol Rhythms 28, 291–300. [PubMed: 23929556]

Brockman R, Bunick D, Mahoney MM, 2011 Estradiol deficiency during development modulates the expression of circadian and daily rhythms in male and female aromatase knockout mice. Hormones and Behavior 60, 439–447. [PubMed: 21816154]

Buhr ED, Takahashi JS, 2013 Molecular components of the mammalian circadian clock. Handbook of experimental pharmacology, 3–27.

Bult A, Hiestand L, Van der Zee EA, Lynch CB, 1993 Circadian rhythms differ between selected mouse lines: a model to study the role of vasopressin neurons in the suprachiasmatic nuclei. Brain Res Bull 32, 623–627. [PubMed: 8221160]

Cheng AH, Fung SW, Cheng HM, 2019 Limitations of the Avp-IRES2-Cre (JAX #023530) and Vip-IRES-Cre (JAX #010908) Models for Chronobiological Investigations. J Biol Rhythms, 748730419871184.

Davidson AJ, Castanon-Cervantes O, Leise TL, Molyneux PC, Harrington ME, 2009 Visualizing jet lag in the mouse suprachiasmatic nucleus and peripheral circadian timing system. Eur J Neurosci 29, 171–180. [PubMed: 19032592]

Edwards MD, Brancaccio M, Chesham JE, Maywood ES, Hastings MH, 2016 Rhythmic expression of cryptochrome induces the circadian clock of arrhythmic suprachiasmatic nuclei through arginine vasopressin signaling. Proc Natl Acad Sci U S A 113, 2732–2737. [PubMed: 26903624]

Evans JA, 2016 Collective timekeeping among cells of the master circadian clock. J Endocrinol 230, R27–49. [PubMed: 27154335]

Evans JA, Gorman MR, 2016 In synch but not in step: Circadian clock circuits regulating plasticity in daily rhythms. Neuroscience 320, 259–280. [PubMed: 26861419]

Evans JA, Leise TL, Castanon-Cervantes O, Davidson AJ, 2011 Intrinsic regulation of spatiotemporal organization within the suprachiasmatic nucleus. PLoS One 6, e15869. [PubMed: 21249213]

Evans JA, Leise TL, Castanon-Cervantes O, Davidson AJ, 2013 Dynamic interactions mediated by nonredundant signaling mechanisms couple circadian clock neurons. Neuron 80, 973–983. [PubMed: 24267653]

Feillet C, Guerin S, Lonchampt M, Dacquet C, Gustafsson JA, Delaunay F, Teboul M, 2016 Sexual dimorphism in circadian physiology is altered in LXRalpha deficient mice. Plos One 11.

Groblewski TA, Nunez AA, Gold RM, 1981 Circadian rhythms in vasopressin deficient rats. Brain Res Bull 6, 125–130. [PubMed: 7470957]

Harris JA, Hirokawa KE, Sorensen SA, Gu H, Mills M, Ng LL, Bohn P, Mortrud M, Ouellette B, Kidney J, Smith KA, Dang C, Sunkin S, Bernard A, Oh SW, Madisen L, Zeng H, 2014 Anatomical characterization of Cre driver mice for neural circuit mapping and manipulation. Frontiers in neural circuits 8, 76. [PubMed: 25071457]

Hastings MH, Maywood ES, Brancaccio M, 2018 Generation of circadian rhythms in the suprachiasmatic nucleus. Nat Rev Neurosci 19, 453–469. [PubMed: 29934559]

Herzog ED, Aton SJ, Numano R, Sakaki Y, Tei H, 2004 Temporal precision in the mammalian circadian system: A reliable clock from less reliable neurons. J Biol Rhythms 19, 35–46. [PubMed: 14964702]

Ingram CD, Snowball RK, Mihai R, 1996 Circadian rhythm of neuronal activity in suprachiasmatic nucleus slices from the vasopressin-deficient Brattleboro rat. Neuroscience 75, 635–641. [PubMed: 8931025]

Iwahana E, Karatsoreos I, Shibata S, Silver R, 2008 Gonadectomy reveals sex differences in circadian rhythms and suprachiasmatic nucleus androgen receptors in mice. Horm Behav 53, 422–430. [PubMed: 18164002]

Kalsbeek A, Fliers E, Hofman MA, Swaab DF, Buijs RM, 2010 Vasopressin and the output of the hypothalamic biological clock. J Neuroendocrinol 22, 362–372. [PubMed: 20088910]

Karatsoreos IN, Butler MP, Lesauter J, Silver R, 2011 Androgens Modulate Structure and Function of the Suprachiasmatic Nucleus Brain Clock. Endocrinology.

Krajnak K, Kashon ML, Rosewell KL, Wise PM, 1998 Sex differences in the daily rhythm of vasoactive intestinal polypeptide but not arginine vasopressin messenger ribonucleic acid in the suprachiasmatic nuclei. Endocrinology 139, 4189–4196. [PubMed: 9751499]

Krizo JA, Mintz EM, 2014 Sex differences in behavioral circadian rhythms in laboratory rodents. Front Endocrinol (Lausanne) 5, 234. [PubMed: 25620955]

Kuljis DA, Loh DH, Truong D, Vosko AM, Ong ML, McClusky R, Arnold AP, Colwell CS, 2013 Gonadal- and sex-chromosome-dependent sex differences in the circadian system. Endocrinology 154, 1501–1512. [PubMed: 23439698]

Li JD, Burton KJ, Zhang C, Hu SB, Zhou QY, 2009 Vasopressin receptor V1a regulates circadian rhythms of locomotor activity and expression of clock-controlled genes in the suprachiasmatic nuclei. Am J Physiol Regul Integr Comp Physiol 296, R824–830. [PubMed: 19052319]

Low-Zeddies SS, Takahashi JS, 2001 Chimera analysis of the *Clock* mutation in mice shows that complex cellular integration determines circadian behavior. Cell 105, 25–42. [PubMed: 11301000]

Ludwig M, 1998 Dendritic release of vasopressin and oxytocin. J Neuroendocrinol 10, 881–895. [PubMed: 9870745]

Mahoney MM, Ramanathan C, Hagenauer MH, Thompson RC, Smale L, Lee T, 2009 Daily rhythms and sex differences in vasoactive intestinal polypeptide, VIPR2 receptor and arginine vasopressin mRNA in the suprachiasmatic nucleus of a diurnal rodent, Arvicanthis niloticus. Eur J Neurosci 30, 1537–1543. [PubMed: 19811536]

Maywood ES, Chesham JE, O'Brien JA, Hastings MH, 2011 A diversity of paracrine signals sustains molecular circadian cycling in suprachiasmatic nucleus circuits. Proc Natl Acad Sci U S A 108, 14306–14311. [PubMed: 21788520]

Mazuski C, Chen SP, Herzog ED, 2020 Different Roles for VIP Neurons in the Neonatal and Adult Suprachiasmatic Nucleus. J Biol Rhythms, 748730420932073.

Meijer JH, Michel S, Vanderleest HT, Rohling JH, 2010 Daily and seasonal adaptation of the circadian clock requires plasticity of the SCN neuronal network. Eur J Neurosci 32, 2143–2151. [PubMed: 21143668]

Mieda M, Okamoto H, Sakurai T, 2016 Manipulating the cellular circadian period of arginine vasopressin neurons alters the behavioral circadian period. Curr Biol 26, 2535–2542. [PubMed: 27568590]

Mieda M, Ono D, Hasegawa E, Okamoto H, Honma K, Honma S, Sakurai T, 2015 Cellular clocks in AVP neurons of the SCN are critical for interneuronal coupling regulating circadian behavior rhythm. Neuron 85, 1103–1116. [PubMed: 25741730]

Ono D, Honma S, Honma K, 2016 Differential roles of AVP and VIP signaling in the postnatal changes of neural networks for coherent circadian rhythms in the SCN. Science advances 2, e1600960. [PubMed: 27626074]

Partch CL, Green CB, Takahashi JS, 2014 Molecular architecture of the mammalian circadian clock. Trends in cell biology 24, 90–99. [PubMed: 23916625]

Prendergast BJ, Onishi KG, Zucker I, 2014 Female mice liberated for inclusion in neuroscience and biomedical research. Neurosci Biobehav Rev 40, 1–5. [PubMed: 24456941]

Rezai Amin S, Gruszczynski C, Guiard BP, Callebert J, Launay JM, Louis F, Betancur C, Vialou V, Gautron S, 2019 Viral vector-mediated Cre recombinase expression in substantia nigra induces lesions of the nigrostriatal pathway associated with perturbations of dopamine-related behaviors and hallmarks of programmed cell death. J Neurochem 150, 330–340. [PubMed: 30748001]

Rigney N, Beaumont R, Petrulis A, 2020a Sex differences in vasopressin 1a receptor regulation of social communication within the lateral habenula and dorsal raphe of mice. Horm Behav 121, 104715. [PubMed: 32067962]

Rigney N, Whylings J, de Vries GJ, Petrulis A, 2020b Sex Differences in the Control of Social Investigation and Anxiety by Vasopressin Cells of the Paraventricular Nucleus of the Hypothalamus. Neuroendocrinology.

Rigney N, Whylings J, Mieda M, de Vries G, Petrulis A, 2019 Sexually Dimorphic Vasopressin Cells Modulate Social Investigation and Communication in Sex-Specific Ways. eNeuro 6.

Rood BD, Stott RT, You S, Smith CJ, Woodbury ME, De Vries GJ, 2013 Site of origin of and sex differences in the vasopressin innervation of the mouse (Mus musculus) brain. J Comp Neurol 521, 2321–2358. [PubMed: 23239101]

Royston SE, Yasui N, Kondilis AG, Lord SV, Katzenellenbogen JA, Mahoney MM, 2014 ESR1 and ESR2 differentially regulate daily and circadian activity rhythms in female mice. Endocrinology 155, 2613–2623. [PubMed: 24735329]

Schwartz WJ, Reppert SM, 1985 Neural regulation of the circadian vasopressin rhythm in cerebrospinal fluid: a pre-eminent role for the suprachiasmatic nuclei. J Neurosci 5, 2771–2778. [PubMed: 4045552]

Smyllie NJ, Chesham JE, Hamnett R, Maywood ES, Hastings MH, 2016 Temporally chimeric mice reveal flexibility of circadian period-setting in the suprachiasmatic nucleus. Proc Natl Acad Sci U S A 113, 3657–3662. [PubMed: 26966234]

Vida B, Deli L, Hrabovszky E, Kalamatianos T, Caraty A, Coen CW, Liposits Z, Kallo I, 2010 Evidence for suprachiasmatic vasopressin neurones innervating kisspeptin neurones in the rostral periventricular area of the mouse brain: regulation by oestrogen. J Neuroendocrinol 22, 1032–1039. [PubMed: 20584108]

Webb AB, Angelo N, Huettner JE, Herzog ED, 2009 Intrinsic, nondeterministic circadian rhythm generation in identified mammalian neurons. Proc Natl Acad Sci U S A 106, 16493–16498. [PubMed: 19805326]

Welsh DK, Logothetis DE, Meister M, Reppert SM, 1995 Individual neurons dissociated from rat suprachiasmatic nucleus express independently phased circadian firing rhythms. Neuron 14, 697–706. [PubMed: 7718233]

Whylings J, Rigney N, Peters NV, de Vries GJ, Petrulis A, 2020 Sexually dimorphic role of BNST vasopressin cells in sickness and social behavior in male and female mice. Brain Behav Immun 83, 68–77. [PubMed: 31550501]

Yamaguchi S, Isejima H, Matsuo T, Okura R, Yagita K, Kobayashi M, Okamura H, 2003 Synchronization of cellular clocks in the suprachiasmatic nucleus. Science 302, 1408–1412. [PubMed: 14631044]

Yamaguchi Y, Suzuki T, Mizoro Y, Kori H, Okada K, Chen Y, Fustin JM, Yamazaki F, Mizuguchi N, Zhang J, Dong X, Tsujimoto G, Okuno Y, Doi M, Okamura H, 2013 Mice genetically deficient in vasopressin V1a and V1b receptors are resistant to jet lag. Science 342, 85–90. [PubMed: 24092737]

Yoo SH, Yamazaki S, Lowrey PL, Shimomura K, Ko CH, Buhr ED, Siepka SM, Hong HK, Oh WJ, Yoo OJ, Menaker M, Takahashi JS, 2004 PERIOD2::LUCIFERASE real-time reporting of circadian dynamics reveals persistent circadian oscillations in mouse peripheral tissues. Proc Natl Acad Sci U S A 101, 5339–5346. [PubMed: 14963227]

Zhang R, Lahens NF, Ballance HI, Hughes ME, Hogenesch JB, 2014 A circadian gene expression atlas in mammals: Implications for biology and medicine. Proc Natl Acad Sci U S A 111, 16219–16224. [PubMed: 25349387]

Highlights

- Vasopressin expression is reduced in the hypothalamus of AVP-IRES-Cre mice
- Vasopressin loss in this model increases water intake and speeds jetlag recovery
- Three novel effects on circadian behavior manifest in a sex-dependent manner
- Phenotypic differences in behavior reflect changes in master clock function
- Clocks constructed differently despite comparable overt rhythms in males and females

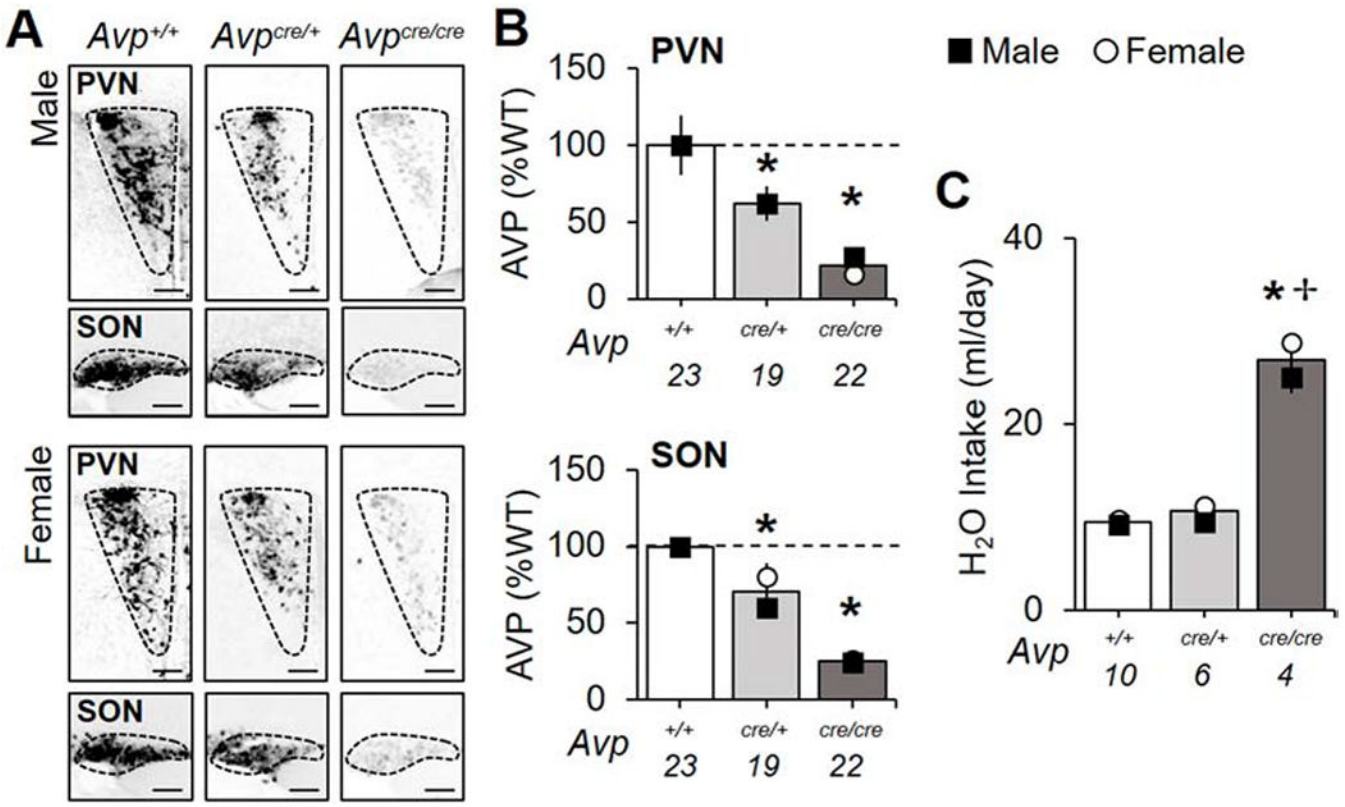

Figure 1.

Decreased AVP and disrupted salt and water balance in $Avp^{cre/cre}$ mice. A. Representative images illustrating AVP levels in the PVN and SON. Scale bar = 100 μm. B. AVP is decreased in the PVN and SON of adult $Avp^{cre/+}$ and $Avp^{cre/cre}$ mice (PVN-Genotype: $F(2,63) = 23.67$, $p < 0.001$, $\eta_p^2 = 0.46$, Sex: $F(1,63) = 0.17$, $p > 0.1$, $\eta_p^2 = 0.003$, Genotype*Sex: $F(2,63) = 0.15$, $p > 0.8$, $\eta_p^2 = 0.003$; SON- Genotype: $F(2,63) = 78.93$, $p < 0.001$, $\eta_p^2 = 0.73$, Sex: $F(1,63) = 2.05$, $p > 0.1$, $\eta_p^2 = 0.03$, Genotype*Sex: $F(2,63) = 1.56$, $p > 0.2$, $\eta_p^2 = 0.05$). For non-normalized values, see Table S1. C. Water consumption is elevated in $Avp^{cre/cre}$ mice (Genotype: $F(2,19) = 202$, $p < 0.001$, $\eta_p^2 = 0.97$, Sex: $F(1,19) = 7.26$, $p < 0.05$, $\eta_p^2 = 0.34$, Genotype*Sex: $F(2,19) = 1.72$, $p > 0.2$, $\eta_p^2 = 0.2$). Numbers below abscissa represent sample size for each genotype, collapsed across sex (A-B: 9-12/sex; C:2-5/sex). Note: small error bars may be obscured by symbols and sex-specific symbols superimposed onto bar graphs may be obscured when female and male data overlap. Post hoc LSM Contrasts: * Differs from $Avp^{+/+}$, genotype difference collapsed across sex, $p < 0.05$, ✣ Sex difference divided by genotype, $p < 0.05$.

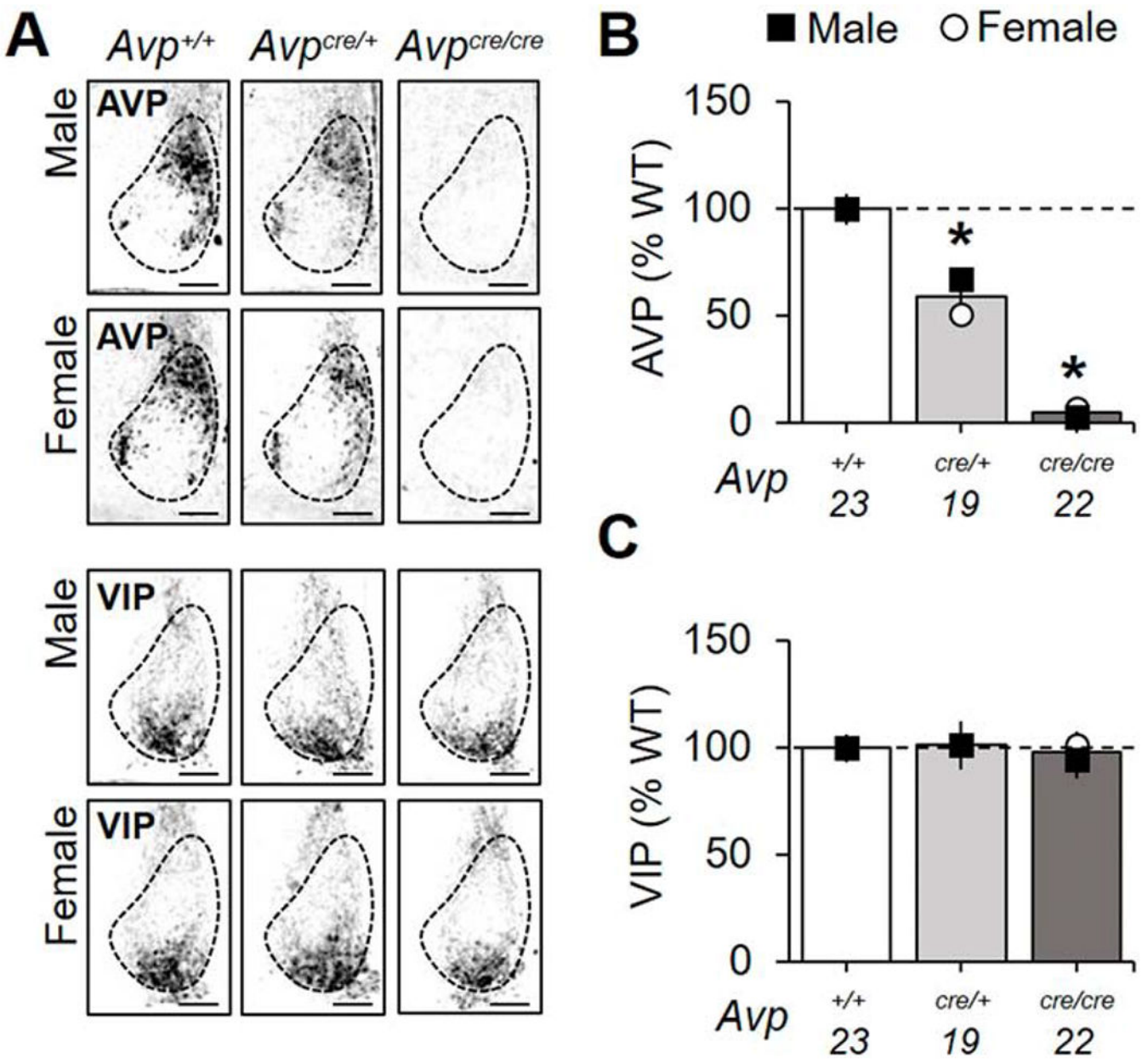

Figure 2.

AVP is decreased in the SCN of $Avp^{cre/+}$ and $Avp^{cre/cre}$ mice, but VIP does not differ. A. Representative images of SCN AVP and VIP expression by genotype and sex. Scale bar = 100 μm. B. SCN AVP is decreased in $Avp^{cre/+}$ and $Avp^{cre/cre}$ mice (Genotype: $F(2,63) = 221$, $p < 0.0001$, $\eta_p^2 = 0.89$, Sex: $F(1,63) = 1.26$, $p > 0.1$, $\eta_p^2 = 0.02$, Genotype*Sex: $F(2,63) = 2.57$, $p = 0.08$, $\eta_p^2 = 0.08$). For non-normalized values, see Table S1. C. SCN VIP does not differ by genotype (Genotype: $F(2,63) = 0.08$, $p > 0.9$, $\eta_p^2 = 0.003$, Sex: $F(1,63) = 0.14$, $p > 0.7$, $\eta_p^2 = 0.002$, Genotype*Sex: $F(2,63) = 0.13$, $p > 0.8$, $\eta_p^2 = 0.005$). Numbers below abscissa represent sample size for each genotype, collapsed across sex (9-12/sex). Post hoc LSM Contrasts: * Differs from $Avp^{+/+}$ genotype difference collapsed across sex, $p < 0.05$, ✣ Sex difference divided by genotype, $p < 0.05$. Other conventions as in Figure 1.

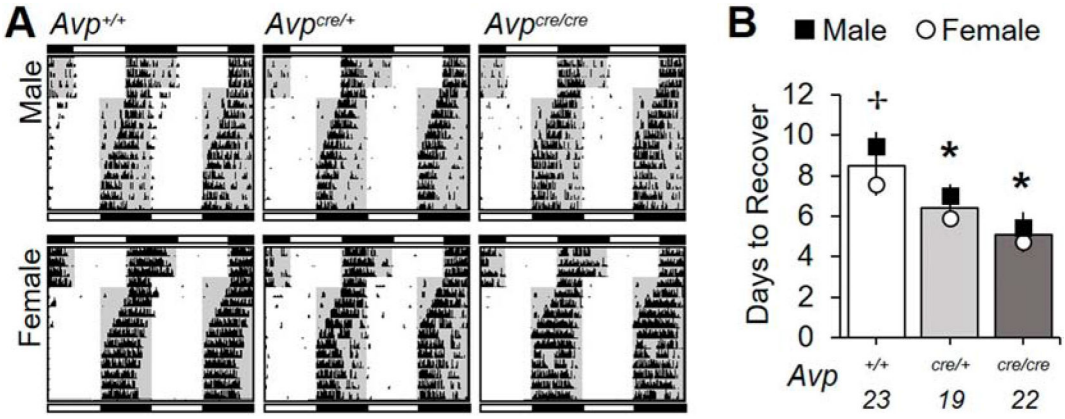

Figure 3.

Recovery from jetlag is accelerated in both $Avp^{cre/+}$ and $Avp^{cre/cre}$ mice. A. Representative double-plotted wheel-running actograms illustrating re-entrainment following the 6 h shift in the light:dark cycle. Lighting conditions before and after the 6 h shift are illustrated with internal shading and light:dark bar above and below each actogram, respectively (black/gray = darkness, white = light). B. $Avp^{cre/+}$ and $Avp^{cre/cre}$ mice re-entrain faster than $Avp^{+/+}$ mice (Genotype: $F(2,63) = 16.7$. $p < 0.001$, $\eta_p^2 = 0.36$, Sex: $F(1,63) = 5.95$, $p < 0.05$, $\eta_p^2 = 0.09$, Genotype*Sex: $F(2,63) = 0.5$, $p > 0.6$, $\eta_p^2 = 0.02$). Numbers below abscissa represent sample size for each genotype, collapsed across sex (9-12/sex). Post hoc LSM Contrasts: * Differs from $Avp^{+/+}$, genotype difference collapsed across sex, $p < 0.05$, ✣ Sex difference divided by genotype, $p < 0.05$. Other conventions as in Figure 1.

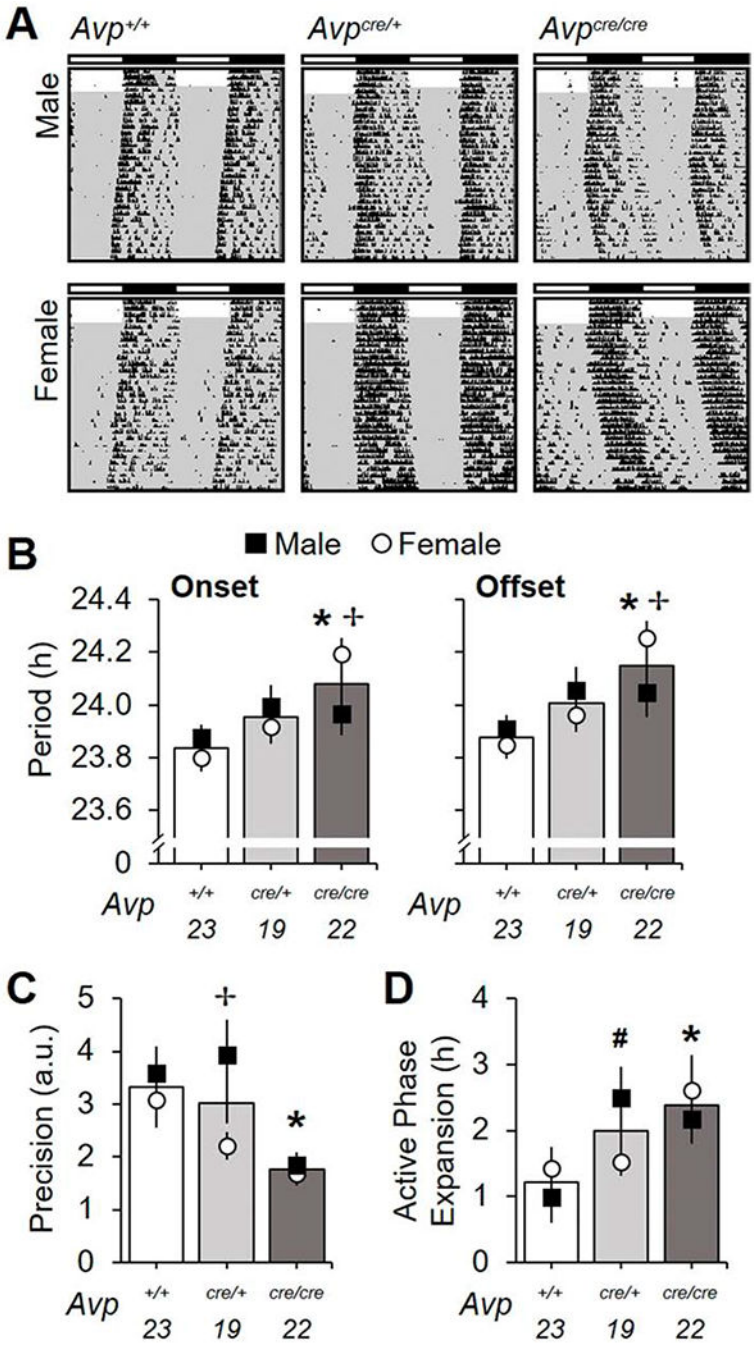

Figure 4.

Avp$^{cre/cre}$ mice display changes in free-running rhythms in constant darkness. A. Representative double-plotted wheel-running actograms illustrating free-running rhythms. Conventions as in Figure 3. B. *Avp*$^{cre/cre}$ mice have longer period length of both activity onset and offset (Onset-Genotype: $F(2,63) = 6.08$, $p < 0.005$, $\eta_p^2 = 0.17$, Sex: $F(1,63) = 0.04$, $p > 0.8$, $\eta_p^2 = 0.0006$, Genotype*Sex: $F(2,63) = 4.167$, $p < 0.005$, $\eta_p^2 = 0.12$; Offset-Genotype: $F(2,63) = 7.71$, $p < 0.001$, $\eta_p^2 = 0.21$, Sex: $F(1,63) = 0.11$, $p > 0.7$, $\eta_p^2 = 0.002$, Genotype*Sex: $F(2,63) = 2.68$, $p = 0.07$, $\eta_p^2 = 0.08$). C. Precision of free-running rhythms

is decreased in $Avp^{cre/cre}$ mice (Genotype: $F(2,63) = 7.28$, $p < 0.0005$, $\eta_p^2 = 0.2$, Sex: $F(1,63) = 4.38$, $p < 0.05$, $\eta_p^2 = 0.07$, Genotype*Sex: $F(2,63) = 1.84$, $p > 0.1$, $\eta_p^2 = 0.06$) D. $Avp^{cre/+}$ and $Avp^{cre/cre}$ mice display larger expansion of the active phase overtime in constant darkness (Genotype: $F(2,63) = 4.97$, $p < 0.01$, $\eta_p^2 = 0.15$, Sex: $F(1,63) = 0.01$, $p > 0.9$, $\eta_p^2 = 0.0002$, Genotype*Sex: $F(2,63) = 2.05$, $p > 0.1$, $\eta_{p2} = 0.07$). Numbers below abscissa represent sample size for each genotype, collapsed across sex (9-12/sex), a.u. = arbitrary units. Post hoc LSM Contrasts: * Differs from $Avp^{+/+}$, genotype difference collapsed across sex, $p < 0.05$, ✣ Sex difference divided by genotype, $p < 0.05$, #Male genotype difference only, $p < 0.05$. Other conventions as in Figure 1.

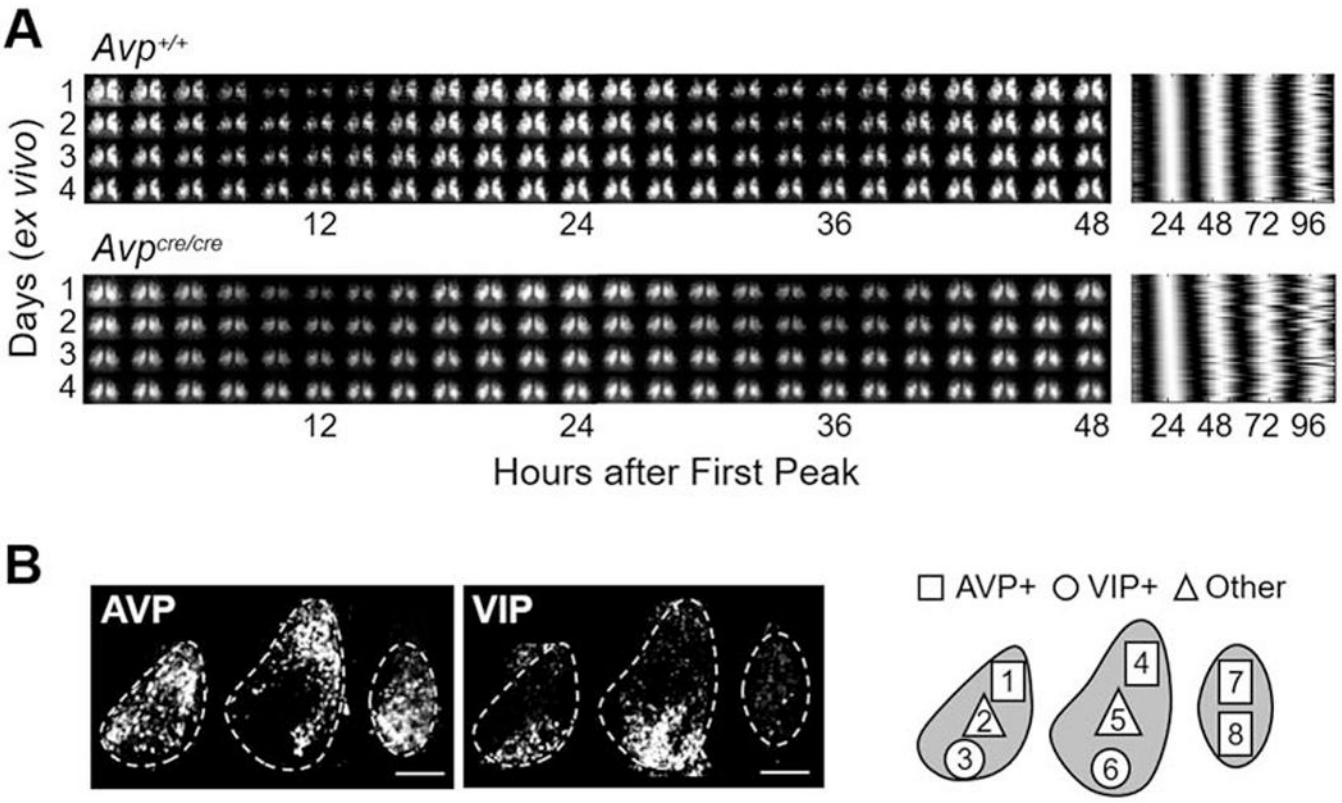

Figure 5.

PER2::LUC rhythms in SCN slices of *Avp*$^{+/+}$ and *Avp*$^{cre/cre}$ mice. A. Representative double-plotted PER2::LUC bioluminescence images in 2 h bins (left) and raster plot illustrating cellular rhythms (right) for middle SCN slices collected from female *Avp*$^{+/+}$ and *Avp*$^{cre/cre}$ mice. B. Representative images illustrating AVP- and VIP-immunoreactivity in PER2::LUC SCN slices. Scale bar = 100 μm. Spatial location of peptidergic regions used for analyses are AVP: 1, 4, 7, 8; VIP:3, 6; Other:2, 5.

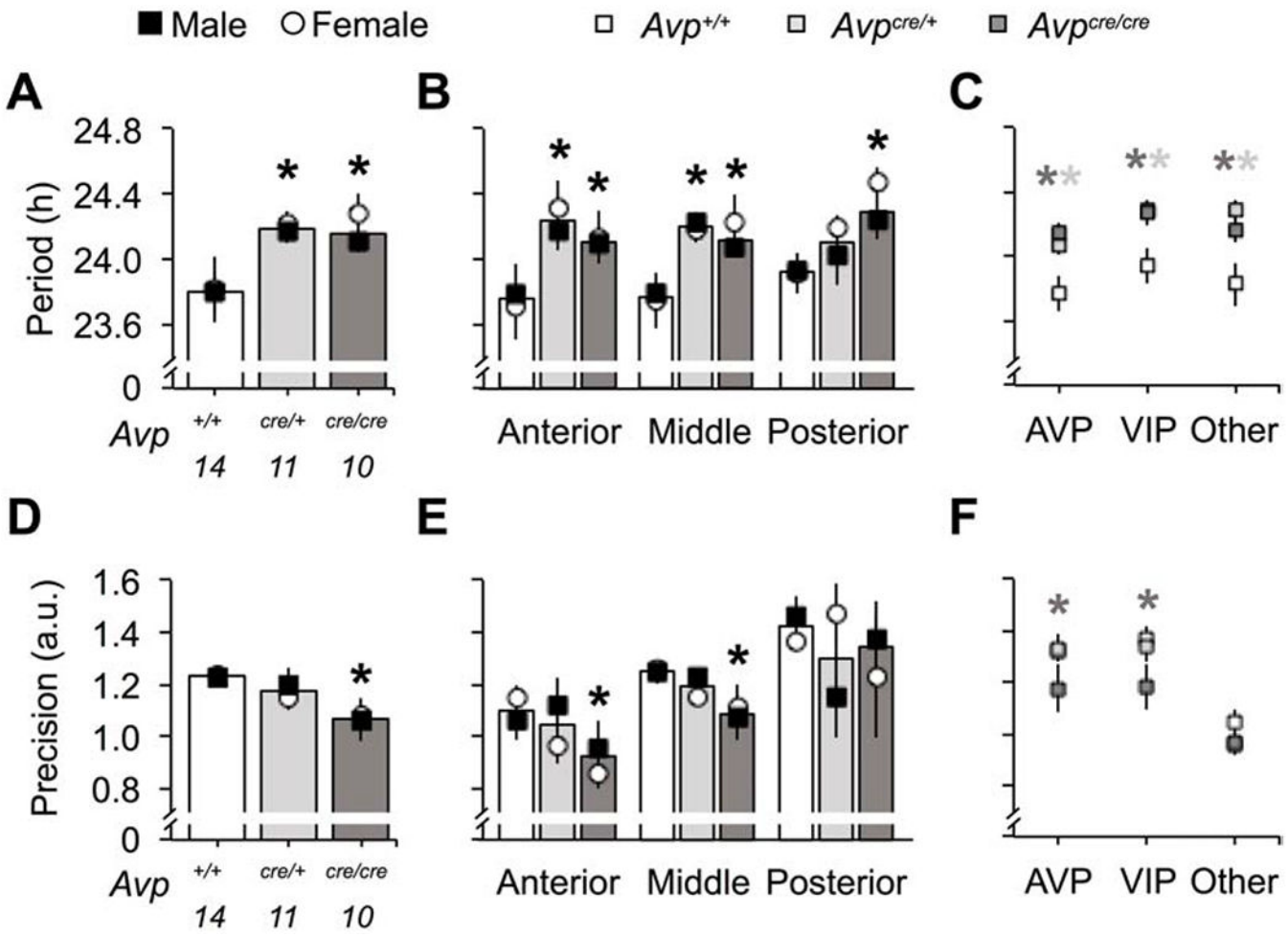

Figure 6.

Avp$^{cre/cre}$ SCN neurons display increased cellular period and decreased cellular precision of PER2::LUC rhythms *ex vivo*. A-C. Cellular period of *Avp*$^{cre/+}$ and *Avp*$^{cre/cre}$ SCN neurons is longer than wild-type (A, Genotype: $F(2,34) = 6.3$, $p < 0.01$, $\eta_p^2 = 0.3$, Sex: $F(1,34) = 0.56$, $p > 0.1$, $\eta_p^2 = 0.02$, Genotype*Sex: $F(2,34) = 0.19$, $p > 0.1$, $\eta_p^2 = 0.01$) across the anteroposterior axis of the network (B, Genotype: $F(2,104) = 10.9$, $p < 0.0001$, $\eta_p^2 = 0.2$, Sex: $F(1,104) = 1.07$, $p > 0.1$, $\eta_p^2 = 0.01$, Slice: $F(2,104) = 0.49$, $p > 0.1$, $\eta_p^2 = 0.01$, Genotype*Sex: $F(2,104) = 0.24$, $p > 0.1$, $\eta_p^2 = 0.006$, Genotype*Slice: $F(4,104) = 0.73$, $p > 0.1$, $\eta_p^2 = 0.03$, Sex*Slice: $F(2,104) = 0.16$, $p > 0.1$, $\eta_p^2 = 0.004$, Genotype*Sex*Slice: $F(4,104) = 0.18$, $p > 0.1$, $\eta_p^2 = 0.008$) and across different peptidergic regions (C, Genotype: $F(2,104) = 13.8$, $p < 0.0001$, $\eta_p^2 = 0.24$, Peptide: $F(2,104) = 1.42$, $p > 0.1$, $\eta_p^2 = 0.03$, Sex: $F(1,104) = 1.29$, $p > 0.1$, $\eta_p^2 = 0.01$, Genotype*Peptide: $F(4,104) = 0.34$, $p > 0.1$, $\eta_p^2 = 0.02$, Genotype*Sex: $F(2,104) = 0.16$, $p > 0.1$, $\eta_p^2 = 0.004$, Peptide*Sex: $F(2,104) = 0.57$, $p > 0.1$, $\eta_p^2 = 0.01$, Genotype*Sex*Peptide: $F(4,104) = 0.45$, $p > 0.1$, $\eta_p^2 = 0.02$). D-F. Cellular precision is decreased in *Avp*$^{cre/cre}$ SCN neurons (D, Genotype: $F(2,34) = 4.09$, $p < 0.05$, $\eta_p^2 = 0.23$, Sex: $F(1,34) = 0.03$, $p > 0.1$, $\eta_p^2 = 0.001$, Genotype*Sex: $F(2,34) = 0.23$, $p > 0.1$, $\eta_p^2 = 0.02$), with regional effects specific to the anterior and middle SCN (E, Genotype: $F(2,104) = 3.68$, $p < 0.05$, $\eta_p^2 = 0.08$, Sex: $F(1,104) = 0.06$, $p > 0.1$, $\eta_p^2 =$

0.0007, Slice: $F(2,104) = 15.68$, $p < 0.0001$, $\eta_p^2 = 0.27$, Genotype*Sex: $F(2,104) = 0.31$, $p > 0.1$, $\eta_p^2 = 0.007$, Genotype*Slice: $F(4,104) = 0.18$, $p > 0.1$, $\eta_p^2 = 0.008$, Sex*Slice: $F(2,104) = 0.24$, $p > 0.1$, $\eta_p^2 = 0.006$, Genotype*Sex*Slice: $F(4,104) = 2.08$, $p = 0.09$, $\eta_p^2 = 0.09$) and to AVP- and VIP-expressing regions (F, Genotype: $F(2,104) = 4.76$, $p < 0.05$, $\eta_p^2 = 0.1$, Peptide: $F(2,104) = 20.91$, $p < 0.0001$, $\eta_p^2 = 0.32$, Sex: $F(1,104) = 1.58$, $p > 0.1$, $\eta_p^2 = 0.02$, Genotype*Peptide: $F(4,104) = 0.97$, $p > 0.1$, $\eta_p^2 = 0.04$, Genotype*Sex: $F(2,104) = 1.12$, $p > 0.1$, $\eta_p^2 = 0.03$, Peptide*Sex: $F(2,104) = 1.2$, $p > 0.1$, $\eta_p^2 = 0.03$, Genotype*Sex*Peptide: $F(4,104) = 1.59$, $p > 0.1$, $\eta_p^2 = 0.07$). Location of peptidergic regions are illustrated in Figure 5. Numbers below abscissa represent sample size for each genotype, collapsed across sex (3-7/sex). a.u. = arbitrary units. Post hoc LSM Contrasts: * Differs from $Avp^{+/+}$, genotype difference collapsed across sex, $p < 0.05$, (color coded for genotype in C and E). Other conventions as in Figure 1.

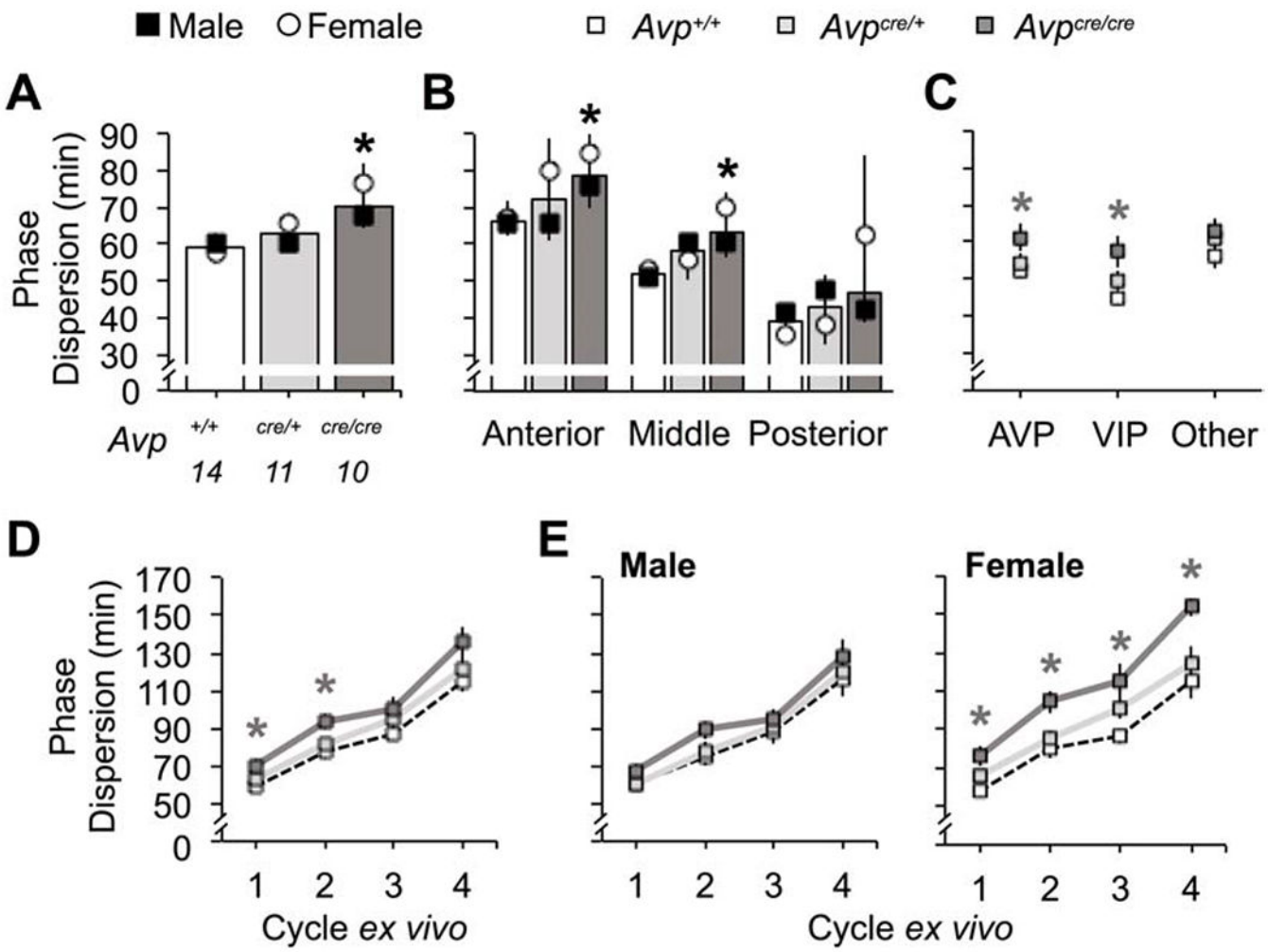

Figure 7.

Avp$^{cre/cre}$ SCN neurons display changes in network organization. A-C. Phase dispersion is increased in *Avp*$^{cre/cre}$ SCN neurons (Genotype: $F(2,34) = 8.23$, $p < 0.005$, $\eta_p^2 = 0.36$, Sex: $F(1,34) = 2.22$, $p > 0.1$, $\eta_p^2 = 0.07$, Genotype*Sex: $F(2,34) = 1.77$, $p > 0.1$, $\eta_p^2 = 0.11$), with regional effects specific to the anterior and middle SCN (B, Genotype: $F(2,104) = 10.68$, $p < 0.001$, $\eta_p^2 = 0.2$, Sex: $F(1,104) = 3.74$, $p = 0.056$, $\eta_p^2 = 0.04$, Slice: $F(2,104) = 51.3$, $p < 0.0001$, $\eta_p^2 = 0.54$, Genotype*Sex: $F(2,104) = 2.82$, $p = 0.06$, $\eta_p^2 = 0.06$, Genotype*Slice: $F(4,104) = 0.17$, $p > 0.1$, $\eta_p^2 = 0.008$, Sex*Slice: $F(2,104) = 0.65$, $p > 0.1$, $\eta_p^2 = 0.01$, Genotype*Sex*Slice: $F(4,104) = 1.47$, $p > 0.1$, $\eta_p^2 = 0.06$) and to AVP- and VIP-expressing regions (C, Genotype: $F(2,104) = 10.68$, $p < 0.001$, $\eta_p^2 = 0.2$, Peptide: $F(2,104) = 5.38$, $p < 0.01$, $\eta_p^2 = 0.11$, Sex: $F(1,104) = 5.11$, $p < 0.05$, $\eta_p^2 = 0.06$, Genotype*Peptide: $F(4,104) = 0.91$, $p > 0.1$, $\eta_p^2 = 0.04$, Genotype*Sex: $F(2,104) = 1.82$, $p > 0.1$, $\eta_p^2 = 0.04$, Peptide*Sex: $F(2,104) = 2.24$, $p > 0.1$, $\eta_p^2 = 0.05$, Genotype*Sex*Peptide: $F(4,104) = 1.69$, $p > 0.1$, $\eta_p^2 = 0.07$). D-E. Phase dispersion overtime is increased in *Avp*$^{cre/cre}$ SCN neurons (Genotype: $F(2,29) = 5.68$, $p < 0.01$, $\eta_p^2 = 0.28$ Sex: $F(1,29) = 3.28$, $p = 0.086$, $\eta_p^2 = 0.1$, Genotype*Sex: $F(2,29) = 1.25$, $p > 0.1$, $\eta_p^2 = 0.08$, Time: $F(3,27) = 92.05$, $p < 0.001$, $\eta_p^2 = 0.88$, Time*Genotype: $F(6,54) = 1.32$, $p >$

0.1, $\eta_p^2 = 0.06$, Time*Sex: $F(3,27) = 1.13$, $p > 0.1$, $\eta_p^2 = 0.02$, Time*Genotype*Sex: $F(6,54) = 0.96$, $p > 0.1$, $\eta_p^2 = 0.04$), due to female-specific effects (E, Male- Genotype: $F(2,18) = 1.02$, $p > 0.1$, $\eta_p^2 = 0.1$, Time: $F(3,16) = 43.47$, $p < 0.0001$, $\eta_p^2 = 0.86$, Genotype*Time: $F(6,32) = 1.32$, $p > 0.1$, $\eta_p^2 = 0.03$; Female-Genotype: $F(2,11) = 6.75$, $p < 0.05$, $\eta_p^2 = 0.55$, Time: $F(3,9) = 61.51$, $p < 0.0001$, $\eta_p^2 = 0.91$, Genotype*Time: $F(6,18) = 1.24$, $p > 0.1$, $\eta_p^2 = 0.19$). Location of peptidergic regions are illustrated in Figure 5. Numbers below abscissa represent sample size for each genotype, collapsed across sex (3-7/sex). Post hoc LSM Contrasts: * Differs from $Avp^{+/+}$. genotype difference collapsed across sex, $p < 0.05$ (color coded for genotype in C-E). Other conventions as in Figure 1.